Journal of Membrane Science 476 (2015) 449–456

Contents lists available at ScienceDirect

Journal of Membrane Science

journal homepage: www.elsevier.com/locate/memsci

Isoporous membranes with gradient porosity by selective swelling of UV-crosslinked block copolymers

Zhaogen Wang, Leiming Guo, Yong Wang*

State Key Laboratory of Materials-Oriented Chemical Engineering, College of Chemistry and Chemical Engineering, Nanjing Tech University, Nanjing 210009, Jiangsu, PR China

ARTICLE INFO

Article history:
Received 9 October 2014
Received in revised form
3 December 2014
Accepted 8 December 2014
Available online 18 December 2014

Keywords:
Block copolymers
Selective swelling
Isoporous membranes
Gradient porosity
pH-responsibility

ABSTRACT

Selective swelling of amphiphilic block copolymers (BCPs) is an effective and nondestructive pore-making strategy. Here we coupled swelling-induced pore generation with UV crosslinking to fabricate BCP isoporous membranes with gradient porosity. Polystyrene-*block*-poly(2-vinylpyridine) (PS-*b*-P2VP) solutions were coated onto macroporous supporting membranes to achieve composite films, which were then annealed in solvent vapor for the perpendicular alignment of the P2VP phases near the surface of the coating BCP layer. After swelling of BCP in hot ethanol and drying, isopores of ~8 nm formed at the surface of BCP layer following the selective swelling-induced pore-formation mechanism. Then UV exposure and subsequent secondary swelling at stronger condition of the membranes were conducted to enlarge the inner pores while maintaining the surface structures. With balanced UV crosslinking and secondary swelling, the finally obtained membranes showed ordered perpendicular pores at the outmost layer and gradient porosity with enlarged interconnected pores inside the BCP layer. Due to the gradient structures, the membranes exhibited much higher flux while the surface structures and retention remained essentially unchanged. Moreover, compared to the membranes without UV treatment, the membranes showed better performances in discriminating polyethylene glycol molecules with different molecular weights and still kept a sensitive pH-responsive property.

1. Introduction

Isoporous membranes possess unique advantages in the precise separation of chemical/biological molecules and particles due to their narrow pore-size distributions [1–4]. A number of isoporous membranes of different materials have been fabricated using various techniques, such as micro/nanofabrication [5], anodization [6], and some improved synthesis processes based on traditional methods [7]. Among these techniques, self-assembly of block copolymers (BCPs) has stood out because of the relatively simple fabrication process and the potential to be upscaled for massive production provided there is affordable supply of BCP materials having acceptable mechanical strength.

BCPs are hybrid molecules comprised of at least two chemically distinct chains of homopolymers which are covalently linked together. Most BCPs undergo phase separation in the microscopic scale, resulting in a number of highly ordered nanostructures [8,9]. Well-defined nanoporous structures will be obtained when transforming the dispersed phases into pores, and this is one of the most frequently used strategies to prepare isoporous membranes from BCPs. Most of the BCPs used for membrane purposes reported so far are polystyrene (PS)-based copolymers and they are not robust enough themselves to survive the pressure applied in the separation processes as PS is a glassy and amorphous polymer with weak mechanical stability although very recently BCPs with substituted PS as the major block have been explored for the purpose of enhanced thermal and chemical stability of the membranes [10]. As a solution to this problem, BCPs are typically used as selective layers composited on a robust macroporous supporting membranes. Yang et al. [11,12] first prepared a thin film of BCP of PS and polymethylmethacrylate (PMMA) on silicon wafers with a sacrificial oxide layer by spin coating, then floated the BCP thin films in water by removing the oxide layer. They collected the floated BCP films on macroporous supports and obtained composite membranes with the BCP layers after they removed the PMMA blocks or PMMA homopolymer premixed in the BCP. This transferring method is effective to make membranes with small areas and have been used by different groups. Alternatively, Phillip et al. [13–15] prepared composite membranes having an isoporous separating BCP layer by directly coating polylactide (PLA)-containing BCPs on water-filled porous supports followed by etching away the labile PLA blocks with alkaline-catalyzed hydrolysis.

* Corresponding author. Tel.: +86 25 8317 2247; fax: +86 25 8317 2292.
E-mail address: yongwang@njtech.edu.cn (Y. Wang).

http://dx.doi.org/10.1016/j.memsci.2014.12.009
0376-7388/

Interestingly, Peinermann et al. reported an elegant method to prepare isoprous membranes by employing nonsolvent-induced phase immersion, which is a mature technique to make polymeric membranes, to block copolymers [16–21]. They obtained asymmetric BCP membranes with highly ordered, thin layers on top of non-ordered sponge-like substructures which had a total thickness of several hundreds of micrometers. This method enjoys foreseeable advantages of upscalablity in the form of either flat sheets [16,17,20] or hollow fibers [19,20] although efforts have to be made to seek cheaper BCP raw materials as the NIPS method which requires concentrated solutions consumes considerably larger amount of BCPs.

In past few years, we developed an alternative approach to make porous BCP membranes on the base of selective swelling-induced pore generation. This approach is highly facile and efficient and nanoporous membranes are produced simply by immersing BCP films in hot solvent, for example, ethanol, and drying them in air [22–24]. Straight pores with monodispersed pores can be achieved if we introduced a solvent annealing process before swelling to perpendicularly align the cylinders of the minority blocks which are transformed to straight pores in the following swelling process [25]. Furthermore, we transferred the aligned BCP thin films onto macroporous polyvinylidene fluoride (PVDF) supporting membranes followed by swelling treatment, and obtained composite membranes with sub-100 nm-thin BCP selective layers [26]. The membranes exhibited high flux and good retention. However, the fabrication process where thin-film transferring is involved is tedious and it might be difficult in terms of large-scale production.

In the present work, we prepare composite membranes having isoporous surface pores and gradient porosity by selective swelling of solvent-annealed BCP films directly coated on macroporous supports. We combine the swelling-induced pore forming and UV crosslinking of BCP to generate gradient porosity. Polystyrene-*block*-poly(2-vinylpyridine) (PS-*b*-P2VP) solutions were coated onto supporting membranes to achieve composite films, which were then annealed in solvent vapor to induce the perpendicular alignment of the P2VP phases near the surface of the coated BCP film. After swelling of BCP and drying, uniform pores of $\sim$8 nm formed at the very surface yet the inner BCP layer consisted of interconnected pores $<$10 nm, which might affect the size-selective separation functions of the surface pores. Subsequently, UV exposure and secondary swelling to a stronger degree of the membranes were conducted to enlarge the inner pores while maintaining the surface structures unchanged. The obtained membranes exhibited much better separation performances than the counterparts without the UV and secondary swelling treatment.

2. Experimental section

2.1. Membrane preparation

Fig. 1 shows the fabrication process for the isoporous membranes with gradient porosity. The BCP, PS-*b*-P2VP, was purchased from Polymer Source and used as received. The numeric molecular weight of the PS and P2VP blocks is 50000 g mol^{-1} and 16,500 g mol^{-1}, respectively, and the PDI of the BCP is 1.09. The BCP coating solution was prepared by dissolving PS-*b*-P2VP in chloroform and the concentration was 2 wt%. PVDF macroporous membranes obtained from Millipore with a pore diameter of 0.22 μm as stated by the manufacturer were served as supports on which the BCP solutions were coated. The coating process was presented in our previous work [24]. Briefly, we carefully spread the BCP solution (10 μl each time) on the surface of PVDF substrate membrane which was prefilled with water, and then dried at 130 °C for 20 min followed by cooling down to room temperature naturally (Fig. 1a). A defect-free and complete coating of the nonporous BCP layer on the supporting membrane was thus obtained as water cannot permeate through the composite film at a pressure of 0.05 MPa. After coating and heat treatment, the film was transferred into an annealing vessel with chloroform inside and the BCP layer was solvent-annealed at room temperature for a certain time (Fig. 1b). Prefilling of the supporting membrane with water was necessary to avoid the BCP layer infiltrating into the pores below during solvent annealing. We then immersed the solvent-annealed film in ethanol at 50 °C for 5 h and a membrane with uniform surface pores was obtained (Fig. 1c). To get gradient porosity under the surface pore, UV crosslinking of the BCP membrane and swelling for the second time under stronger swelling conditions (secondary swelling) were used. The membrane was exposed to UV light with a wavelength of 254 nm at the intensity of 1 mW/cm^2 for 2 min to fix the porous structure on the surface (Fig. 1d) and then swollen in ethanol to a larger degree at pre-determined temperatures for different durations (Fig. 1e). Thus a composite membrane composed of a PVDF supporting layer and an isoporous BCP selective layer with gradient porosity were obtained.

2.2. Characterizations

We used scanning electron microscopy (SEM) to characterize the morphology of the membranes. SEM images of surfaces and cross sections of the samples were taken on a field-emission microscope (Hitachi S4800) operated at 5.0 keV. Before SEM observations, the samples were sputtering coated with an ultrathin layer of Pt/Pd alloy to avoid charging. X-ray photoelectron spectroscopy (XPS) characterizations were carried out on a Thermo Scientific ESCALAB 250 XPS system using monochromatic Al Kα as the X-ray source and the electron take-off angle was set at 0°.

2.3. Filtration experiments

Flux and separation experiments were carried out in a Millipore Amicon 8010 stirred filtration cell. The membranes were prepressed at the pressure of 0.05 MPa for 10 min prior to the filtration tests. Bovine serum albumin (BSA) with purity higher than 97% was purchased from General Material. BSA was dissolved in phosphate buffered solution (PBS, pH 7.4) at the concentration of 0.5 g/L. The concentrations of BSA were determined from the UV absorbance at 280 nm with a Thermo minitype UV–vis absorption Spectrometer (NanoDrop 2000c). A mixed solution (total concentration 0.6 g/L) of two equal polyethylene glycol (PEG, PDI $<$1.10, purchased from Polymer Source Inc.) with the molecular weights of 22 kDa and 102 kDa in water was used to test the size-sieving property of the membranes, and the filtration of PEG was analyzed via gel permeation chromatography (GPC, Waters 1515).

We tested the fluxes of water with different pH values (2–9) of the membranes to illustrate their pH-responsive property. Firstly, one composite membrane was kept in a beaker with water (pH=2) for 30 min, allowing the P2VP chains to swell completely. The wet membrane was then placed in the stirred cell module and the flux of water (pH=2) was measured. Note that a 10-min prepressing of the membrane at 0.05 MPa was applied before every measurement. After that, the cell module was cleaned carefully and rinsed with water at a pH=3 for several times, and the membrane was immersed in water (pH=3) for 30 min and its flux of water (pH=3) was then measured. The flux of water (pH from 2 to 9 and then 9 to 2) of the composite membrane was measured in the same way.

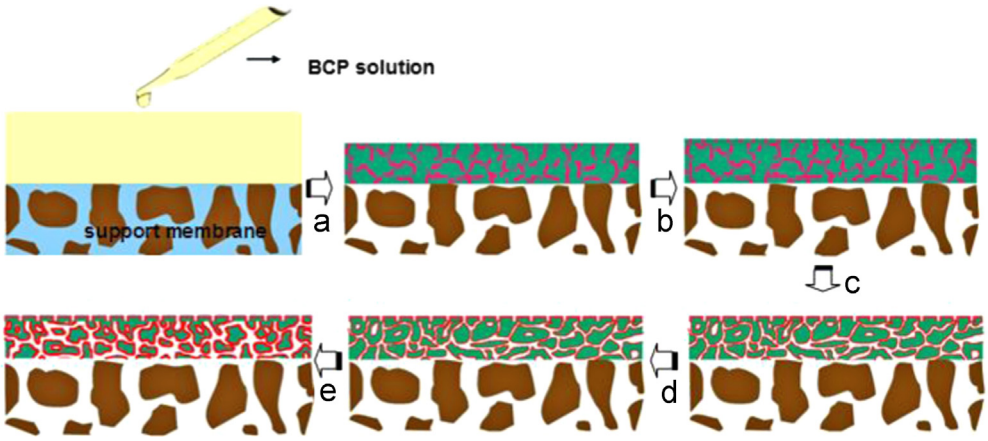

Fig. 1. Schematic of the preparation of the isoporous membrane with gradient porosity. (a) BCP layer coating, (b) the perpendicular alignment by solvent annealing, (c) pore-making by swelling in ethanol, (d) surface crosslinking by UV exposure, and (e) enlarging of the inner pores and producing the gradient porosity by secondary swelling at a stronger swelling conditions.

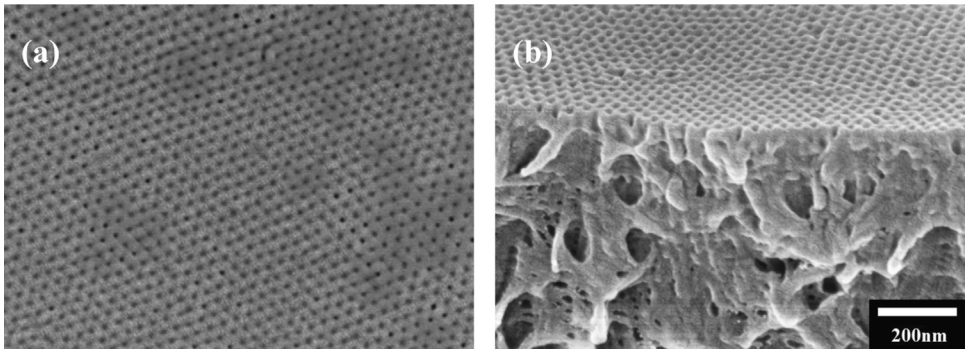

Fig. 2. SEM images of the BCP layer after solvent annealing and ethanol swelling: (a) surface and (b) cross section. Both panels have the identical magnification and the scale bar is found in panel (b).

3. Results and discussions

Pore size distribution and other surface properties are key factors affecting membrane performances [27,28]. Generally, a porous membrane with a narrower pore size distribution can show better size-sieving property. In our previous work, composite membranes consisting of a mesoporous BCP layer and a macroporous support layer were fabricated [24]. The interconnected pores in BCP layer were structured, yet far from uniform. To further improve the pore regularity and thus narrow the pore size distribution, we took solvent annealing to adjust the microphase separation and achieve a highly ordered perpendicular alignment of the PS-*b*-P2VP film. The BCP film was annealed in the saturated vapor of chloroform. It was found that short annealing in a neutral solvent followed by instant solvent evaporation produced a highly ordered perpendicularly aligned morphology. The solvent-annealed PS-*b*-P2VP film was then swollen in ethanol at 50 °C for 5 h and dried in air, and uniform pores with a diameter ~8.0 nm were formed (Fig. 2a), following the pore forming mechanism of selective swelling. However, the cross-sectional SEM images showed that the inner PS-*b*-P2VP layer was made up of interconnected pores with a diameter less than 10 nm (Figs. 2b and S1), and these inner pores affect the permeability of the membrane as well as size-selective separation functions of the surface pores as the pore sizes of the inner pores are comparable to the surface pores, for instance, such a membrane gave a very low water flux (80 L/(m^2 h bar)). Both the uniform surface pores and the interconnected pores underneath the surface play a role in determining the size-sieving performance of the membranes.

One common strategy to solve this problem is to lower down the thickness of the selective layer and therefore to reduce the transport resistance produced by the pores underneath. There are two existing routes realizing thin selective layer: one is to directly spin-coat the BCP solution onto the supporting membrane [15], the other is the sacrificial layer method [11,26,29]. Nanoporous membranes with top BCP layer lower than 500 nm can be obtained via both methods. However, as we already mentioned in Section 1 it is challenging to produce composite membranes with large areas using both methods. Alternatively, we propose a two-step fabrication strategy: maintaining the isoporous surface unchanged and enlarging the inner pores.

UV exposure of the annealed and swelling-treated composite membranes was utilized to fixate PS and P2VP chains on the surface by crosslinking [30] and thus maintain the surface isoporous structure during the secondary swelling. UV exposure can induce both crosslinking and degradation in polymer films, so an appropriate UV dosage is crucial. A UV intensity of 1 mW/cm^2 for 2 min in air was used here. Upon UV exposure, radical species were produced on the PS and P2VP chains, which then recombined to generate a crosslinked network. In addition, UV exposure is a thickness-dependent process and it will result a progressively reduced degree of crosslinking from the top surface to the interior of the polymer film. Therefore, we could significantly crosslink the polymer chains in the top surface on which the UV light was directly shed while barely disturbing the polymer chains in the interior within a relatively short exposure time. The surface morphology of the annealed and swelling-treated composite membrane was preserved after UV exposure (Fig. S2). XPS analysis also showed that the compositions of the PS-*b*-P2VP layer did not

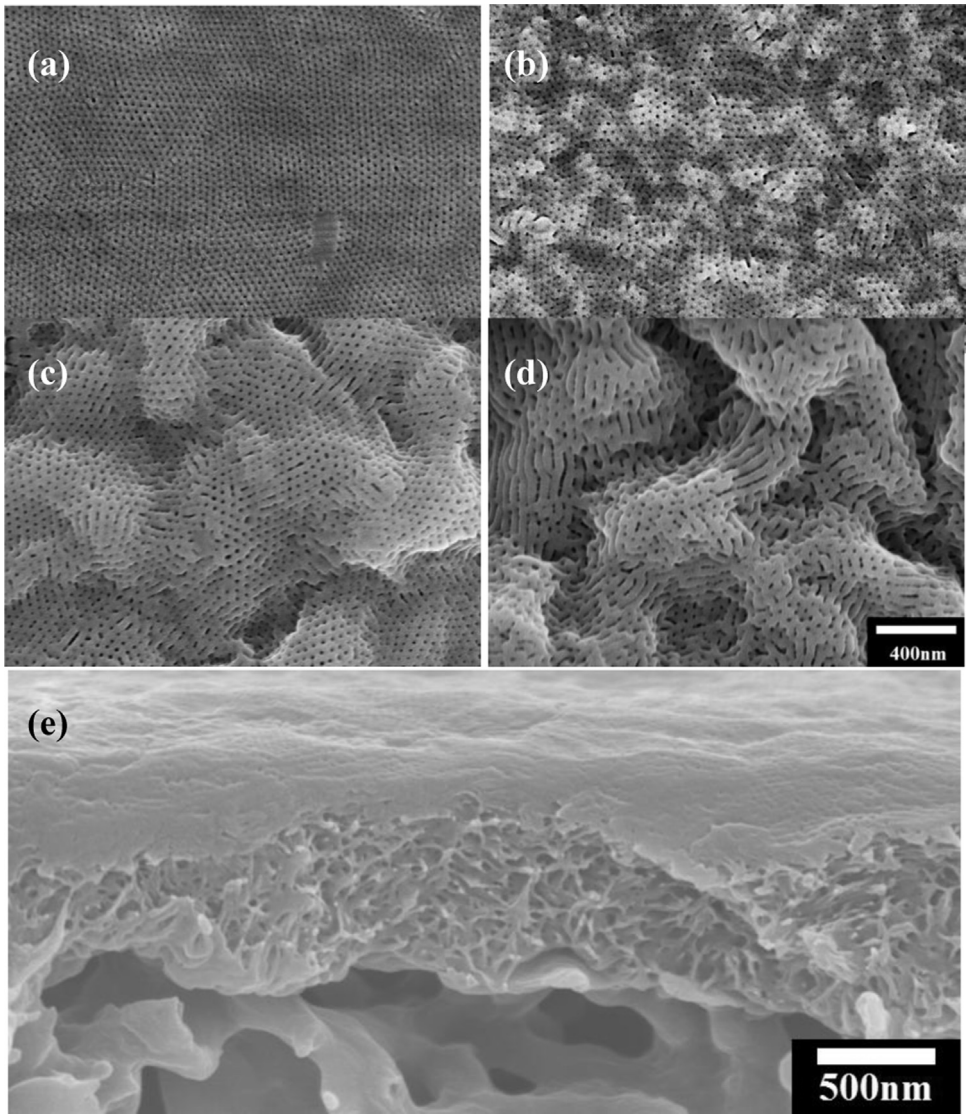

Fig. 3. (a–d) Surface SEM images of the composite membranes which were subjected to UV treatment and secondary swelling at stronger but different swelling conditions: (a) 60 °C for 1 h, (b) 60 °C for 5 h, (c) 60 °C for 15 h, and (d) 70 °C for 5 h. (e) The cross-sectional morphology of (a). (a–d) shows the identical magnification and the scale bar is placed in panel (d).

change evidently with UV exposure (Fig. 4). In contrast, if the UV dosage was not proper (Fig. S3a) or the exposure time was too long (Fig. S3b), cracks or pore blocking emerged.

After UV exposure, the sample was immersed in hot ethanol subjected to secondary swelling to a stronger degree to enlarge the pores inside the BCP layer. The degree of swelling was significantly influenced by the swelling temperature and swelling time. Higher swelling temperature or longer swelling time can lead to a stronger deformation degree of both the PS matrix and the P2VP chains during the swelling process and, consequently larger pores [23,25]. So the diameters of the inner pores increased after secondary swelling. However, due to the UV crosslinking, the mobility of the surface polymer chains was reduced severely and the isoporous structure at the surface was maintained. As a result, an isoporous membrane with gradient porosity was obtained. We investigated the surface morphologies of the UV treated membranes subjected to secondary swelling at different swelling conditions. SEM image in Fig. 3a revealed that the composite membrane after UV exposure and secondary swelling in 60 °C ethanol for 1 h showed highly ordered circular pores with a diameter of ~8.1 nm which was consistent with the membrane before UV exposure. In contrast, if the annealed and swelling-treated composite membrane was directly swelled in 60 °C ethanol for 1 h without UV exposure, its initially ordered alignment ruined and the membrane showed a twisted and interconnected pore structure with a pore diameter >13 nm (Fig. S4a), much like that of the membrane swelling at 60 °C for 1 h without a prior solvent annealing (Fig. S4b). That is, for the UV-treated membrane, the UV-crosslinked surface polymer chains were restricted so its surface structures were not disturbed by the following secondary swelling. On the contrary, the surface morphology of the membrane without UV exposure was changed by secondary swelling as the polymer chains were mobile and able to deform under further swelling treatment.

When we did the swelling at 60 °C for 5 h, the membrane surface was slightly waved as shown in Fig. 3b, which was due to a confliction between the enlarged inner pores and the limited space determined by the supporting membrane. However, as the UV-crosslinked polymer chains on the surface were restricted, the pores on the surface still kept a highly ordered and uniform state and the mean pore diameter was ~8.3 nm, much the same with that before UV exposure. The surfaces became more waved when we further increased the swelling condition at 60 °C for 15 h, and the mean pore diameter increased to ~10.2 nm (Fig. 3c). The gradually changing morphologies indicated a competition between

the tendency to preserve the structure endowed by UV crosslinking and the tendency to enlarge the pore induced by secondary swelling. In spite of the waved surface and the increasing pore sizes, the isoporous structure on the membrane surface was preserved, indicating that the structure-preserving tendency endowed by UV crosslinking of polymer chains still played a major role. As mentioned, temperature is a crucial factor in the swelling process and higher swelling temperature leads to higher degree of swelling and consequently larger pores. We also observed the surface morphology of the UV-exposed membrane subjected to secondary swelling in 70 °C for 5 h as shown in Fig. 3d. The membrane surface was waved to an even stronger extent and the mean pore diameter increased to ~14.3 nm. Moreover, some initially cylindrical pores merged with neighboring ones and converted to channel-like pores. It indicated that the secondary swelling induced structural transformation prevailed in its competition with the structure-preserving tendency endowed by UV exposure. Fig. 3e showed the cross-sectional morphology of the membrane after UV exposure and following secondary swelling in ethanol at 60 °C for 1 h. It is clear that the membrane was composed of three gradient layers: the top isoporous layer with a pore diameter < 10 nm and thickness < 100 nm, the lower gradient BCP layer with larger interconnected pores and the supporting macroporous layer. Compared to the membrane which did not receive UV treatment (Fig. 2b), the membrane subjected to UV treatment and secondary swelling exhibited larger inner BCP pores and a gradient porosity. As a result, the filtration resistance of such membranes with gradient porosity and larger pores will be reduced and a better permeability as well as size-selective separation function was expected.

XPS was used to reveal the chemical compositions of the PS-*b*-P2VP surface layer of the composite membranes prepared under different conditions. And the nitrogen to carbon (N/C) atomic ratios were used to indicate the relative concentrations of P2VP on the top surface of membranes, as shown in Fig. 4. The surface N/C ratio of the annealed and swelling-treated membrane, the membrane further subjected to UV exposure, and the membrane further subjected to secondary swelling at UV-60 °C for 1 h was 5.39%, 5.67%, and 5.56%, respectively. The nearly identical N/C ratios within the measurement errors indicated nearly the same surface P2VP contents and therefore confirmed the retaining of the surface structure during UV exposure and the following secondary swelling at 60 °C for 1 h. When the secondary swelling was carried out at 60 °C for 15 h, the surface N/C ratio of the membrane noticeably increased to 8.23%. This was because more P2VP moieties translocated to the surface as the surface retaining endowed by UV crosslinking could not completely prevent the structural transformation forced by secondary swelling last for longer time.

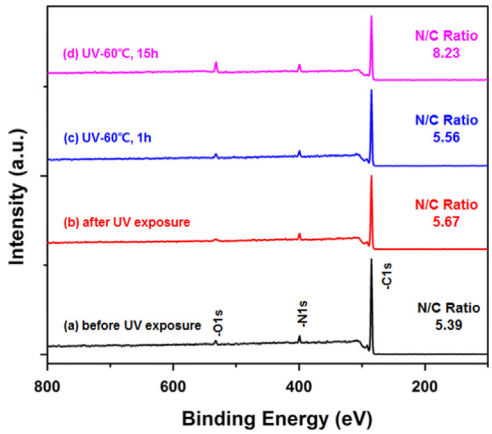

Fig. 4. XPS wide-scan spectra of (a) the annealed and swelling-treated membrane, (b) the membrane further subjected to UV exposure, and (c) the membrane further subjected to secondary swelling at UV-60 °C for 1 h and (d) 15 h.

We then studied the permeability and retention performances of membranes prepared under different conditions, and the results are illustrated in Fig. 5. *Membr*. 1 referred to the annealed and swelling-treated membrane without UV exposure. It showed a pure water flux of 83 L/(m^2 h bar) and a rejection of 95.6% to BSA as both the pores on the surface and in the interior were less than 10 nm, which would be smaller when used due to slight swelling of PS-*b*-P2VP in water. *Membr*. 2 and *Membr*. 3 referred to the membrane subjected to UV exposure and secondary swelling at 60 °C for 1 h and 15 h, respectively. After UV exposure and secondary swelling, the membrane exhibited much better permeability. For *Membr*. 2, the pure water flux was 295 L/(m^2 h bar), more than three times larger than that of *Membr*. 1, while the BSA retention maintained at 94.7%. As mentioned above, for the annealed and swelling-treated membrane, the surface structure was well kept and the inner BCP pores were enlarged after UV crosslinking and subsequent secondary swelling at 60 °C for 1 h. The highly ordered surface pores with a diameter ~8.3 nm played a decisive role in rejecting BSA, and the enlarged inner pores contributed to reducing of the membrane mass-transfer resistance and thus improving of the permeability. When the secondary swelling at 60 °C increased to 15 h, the membrane showed a pure water flux of 557 L/(m^2 h bar) and a BSA retention of 93.4%. The flux was almost seven times higher than that of *Membr*. 1 while the BSA retention barely declined. This was because swelling at 60 °C for 15 h induced much larger inner pores and on the other hand, the 10-nm ordered pores could still reject BSA efficiently in water. *Membr*. 4 and *Membr*. 5 were the control samples subjected only to ethanol swelling at 60 °C for 1 h and 15 h, respectively and no solvent annealing, UV treatment or secondary annealing was carried on them. The water flux of *Membr*. 4 and *Membr*. 5 was 391 L/(m^2 h bar) and 788 L/(m^2 h bar), the BSA retention 59.4% and 47.4%, respectively. Compared to *Membr*. 4, *Membr*. 3 which was secondarily swelled at 60 °C for 15 h exhibited both higher flux and retention because of the gradient porosity and larger pores.

Membrane resistance analysis was conducted to further illustrate the gradient porosity of the composite membranes. The filtration resistance from membrane itself R_m was calculated using the Darcy filtration model [31]

$$J_0 = \frac{\Delta P}{\mu R_m} \quad (1)$$

where ΔP is the pressure drop across a membrane, μ is the water viscosity, 0.89×10^{-3} Pa s, and J_0 is the pure water flux. Therefore, the membrane resistance can be estimated just from the pure

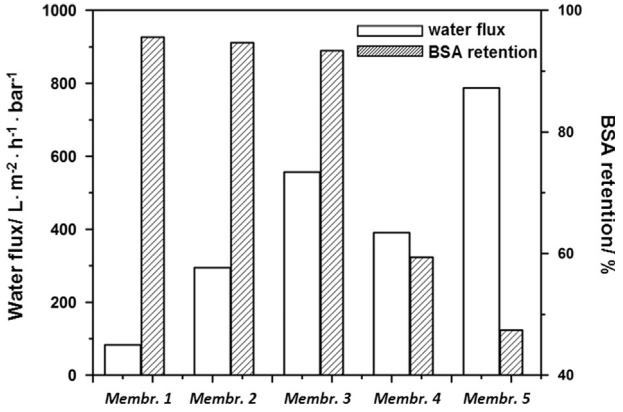

Fig. 5. The water flux and BSA rentention of different membranes. *Membr*. 1: annealed and swelling-treated membrane without UV exposure; *Membr*. 2 and *Membr*. 3: the membrane subjected to UV exposure and secondary swelling at 60 °C for 1 h and 15 h, respectively; *Membr*. 4 and *Membr*. 5: the membranes which were only swollen in ethanol at 60 °C for 1 h and 15 h, respectively and no solvent annealing, UV treatment or secondary annealing was carried on them.

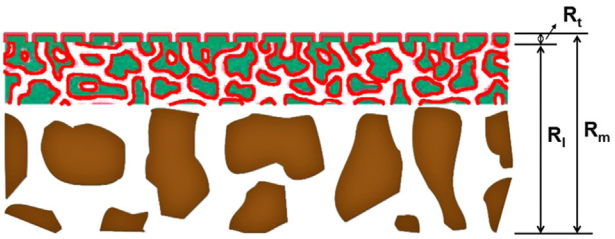

Fig. 6. The schematic depiction of the analysis of membrane resistance.

Table 1
Membrane resistance values of membranes before and after the treatment of UV exposure and secondary swelling at 60 °C for 1 h.

	R_t (m^{-1})	R_l (m^{-1})	R_m (m^{-1})	R_t/R_m (%)
Before	3.10×10^{11}	45.0×10^{11}	48.1×10^{11}	6.44
After	3.10×10^{11}	10.5×10^{11}	13.6×10^{11}	22.8

water flux. We compared the integral membrane resistance R_m, the top isoporous layer resistance R_t, and the lower subsurface layer (including the gradient BCP layer and the supporting macroporous layer) resistance R_l (Fig. 6) of the annealed and swelling-treated membrane before and after UV exposure and secondary swelling at 60 °C for 1 h. For the annealed and swelling-treated membrane before UV exposure and secondary swelling (namely, *Membr*. 1), R_m was calculated according to its pure water flux, and R_l was calculated according to the pure water flux of the membrane subjected only to ethanol swelling at 50 °C for 5 h and no solvent annealing, which had a structure similar to that of the lower subsurface layer of *Membr*. 1. R_t was the subtraction of R_l from R_m. For the annealed and swelling-treated membrane after UV exposure and secondary swelling (namely, *Membr*. 2), R_m was also calculated according to its pure water flux. *Membr*. 1 and *Membr*. 2 had a same R_t as they showed similar top layer structures, and R_l was the subtraction of R_t from R_m. As shown in Table 1, the membrane before such treatment exhibited a much higher membrane resistance than the treated one because of the more than four times higher resistance from the layer underneath the surface layer. We can also conclude from the table that the resistance for the membrane without UV exposure and secondary swelling is mainly from the subsurface layer and the resistance from the surface layer can be neglected because it only accounted for 6.44%. In contrast, for the membrane subjected to UV exposure and secondary swelling, the role of the surface layer became evident as it was accounted for 22.8% to the whole membrane resistance.

Two PEG molecules with molecular weights of 22 KDa and 102 KDa, respectively were used to investigate the size-sieving performances of the composite membranes. GPC curves are shown in Fig. 7. The annealed and swelling-treated membrane before UV exposure displayed a retention of 40.9% and 83.3% to 22 KDa and 102 KDa PEG, respectively. While for the membrane after secondary swelling at 60 °C for 1 h, the retention was 31.8% and 86.5%, respectively, and for the membrane after secondary swelling at 60 °C for 15 h, the retention was 17.2% and 85.2%, respectively. It indicates that after UV exposure and secondary swelling the membrane kept almost the same retention to larger PEG molecules and it exhibited less retention to the smaller PEG molecules because the subsurface layer in the membrane receiving no UV exposure and secondary swelling also delivered a retention function. The separation factors to 22 KDa and 102 KDa PEG of the above-mentioned three membranes were 2.04, 2.72 and 4.95, respectively. That is, the membrane subjected to UV exposure and secondary swelling behaved better in discriminating the two PEG molecules and moreover, the membrane with 15 h secondary swelling worked even better than the one with 1 h secondary swelling.

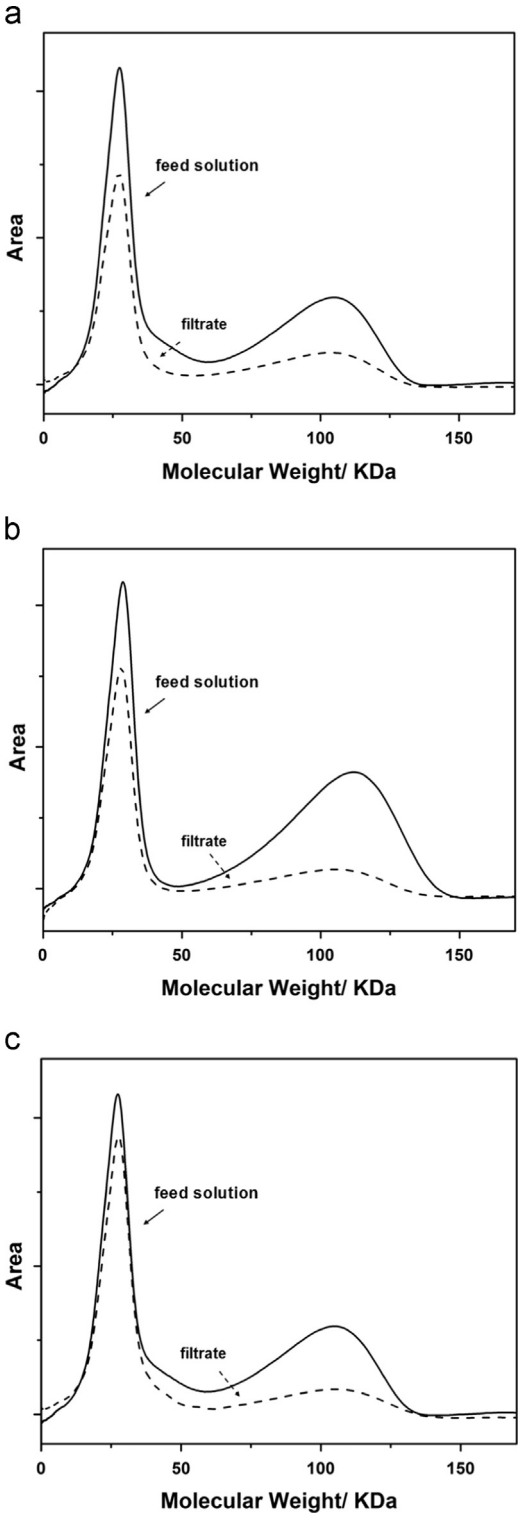

Fig. 7. GPC curves showing the selective sieving to 22 KDa and 102 KDa PEG molecules of (a) the annealed and swelling-treated membrane before UV exposure, the membrane subjected to UV exposure and secondary swelling at 60 °C for 1 h (b) and for 15 h (c).

The membranes subjected to UV exposure and secondary swelling also showed a pH-responsive property although the

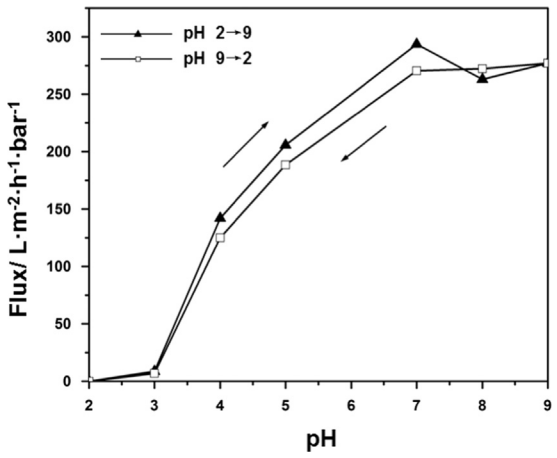

Fig. 8. Water flux of the membrane subjected to secondary swelling at 60 °C for 1 h as a function of pH.

P2VP segments migrated on the pore wall were crosslinked by UV exposure. We tested the water flux of the membrane subjected to secondary swelling at 60 °C for 1 h under different pH values and the results are shown in Fig. 8. When pH was lower than 2, no water permeated the membrane. The membrane pores were considered to be closed. The flux showed an increase of more than 1 order of magnitude when the pH changed from 3 to 7. Then the flux decreased slightly with the increase of pH till 9. Furthermore, the change of water flux as a function of pH was reversible. When pH decreased, the nitrogen atoms on P2VP chains performed stronger protonation. And P2VP chains stretched to a larger extent because of the electrostatic exclusion, resulting in a decrease of effective pore size of BCP layer and thus the decrease of water flux at the macroscopic level [32,33]. When the pH was switched from 7 to 3, around the isoelectric point of P2VP, protonation between the nitrogen atoms took place at a stronger degree and the flux showed a sharp decrease. When the pH decreased to 2, stretched P2VP chains had already covered the nanopores on the surface. Reversibility of protonation between the nitrogen atoms as a function of pH led to the reversibility of the change of water flux. Such a pH-dependent permeability of the UV-treated membrane was similar, both in the trend and the amplitude of the flux change, to the membrane made of the same BCP but subjected to no UV crosslinking [24]. On the membrane surface the P2VP chains were expected to be significantly crosslinked and their change in conformation with varying pH might be restricted to some extent. However, the P2VP chains in the bottom part of the BCP layer were slightly influenced or not at all by UV exposure and they changed their conformations to respond the changes in pH and resulted in an evident pH-dependent permeability.

4. Conclusions

Block-copolymer-based isoporous membranes with gradient porosity are prepared. Dilute solutions of PS-*b*-P2VP were directly coated on the surface of macroporous PVDF substrate membranes and a solvent annealing process was applied to induce the perpendicular orientation of P2VP cylinders on the BCP surface. The annealed BCP film composited on PVDF support was then immersed in hot ethanol to make isopores on the surface and interconnected pores inside the BCP layer following the pore generation mechanism of selective swelling. The BCP layer was exposed to UV light shortly and the BCP chains were crosslinked with a progressively reduced degree of crosslinking. We then applied a secondary swelling in ethanol to the UV-exposed BCP membrane at stronger swelling conditions. We obtained BCP separating layer with isoporous surface pores and gradient porosity because the secondary swelling did not change the isoporous structure on the surface as the BCP chains were largely fixated by UV crosslinking and enlarged the pores inside the BCP layer as the crosslinking became gradually weak at deeper positions. Cross-sectional SEM observation and membrane resistance analysis confirmed the gradient porosity in the BCP layer. The resulting membranes showed higher permeability by a factor of three to seven at no expense of retention compared to membranes subjected to no treatment of UV exposure and secondary swelling. Moreover, such membranes exhibited better performances in discriminating polyethylene glycol molecules with different molecular weights. Additionally, we found that the membrane kept its smart nature to respond to the change toward varying pH and the UV exposure did not noticeably hurt the pH-responsive property of the membrane as the P2VP chains especially in the bottom part in the BCP layer were not fully locked by the UV crosslinking.

Acknowledgments

Financial support from the National Basic Research Program of China (2015CB655301), the Fok Ying Dong Education Foundation (131046), the Jiangsu Natural Science Funds for Distinguished Young Scholars (BK2012039), and the Project of Priority Academic Program Development of Jiangsu Higher Education Institutions (PAPD) is gratefully acknowledged.

Appendix A. Supporting information

Supplementary data associated with this article can be found in the online version at http://dx.doi.org/10.1016/j.memsci.2014.12.009.

References

[1] C. Van Rijn, Nano and Micro Engineered Membrane Technology, Elsevier science, Amsterdam, The Netherlands, 2004.
[2] C.C. Striemer, T.R. Gaborski, J.L. McGrath, P.M. Fauchet, Charge- and size-based separation of macromolecules using ultrathin silicon membranes, Nature 445 (7129) (2007) 749–753.
[3] S.Y. Yang, J.A. Yang, E.S. Kim, G. Jeon, E.J. Oh, K.Y. Choi, S.K. Hahn, J.K. Kim, Single-file diffusion of protein drugs through cylindrical nanochannels, ACS Nano 4 (7) (2010) 3817–3822.
[4] Y.K. Choi, S.M. Park, S. Lee, D.Y. Khang, D.C. Choi, C.H. Lee, Characterization and theoretical analysis of isoporous cycloaliphatic polyurethane membrane for water treatment, Desalin. Water Treat. 52 (4–6) (2014) 1021–1027.
[5] H. Mukaibo, L.P. Horne, D. Park, C.R. Martin, Controlling the length of conical pores etched in ion-tracked poly-(ethylene terephthalate) membranes, Small 5 (21) (2009) 2474–2479.
[6] R.C. Furneaux, W.R. Rigby, A.P. Davidson, The formation of controlled-porosity membranes from anodically oxidized aluminium, Nature 337 (6203) (1989) 147–149.
[7] M. Warkiani, A. Bhagat, B. Khoo, J. Han, C. Lim, H. Gong, A. Fane, Isoporous micro/nanoengineered membranes, ACS Nano 7 (3) (2013) 1882–1904.
[8] R.A. Segalman, Patterning with block copolymer thin films, Mater. Sci. Eng. R 48 (6) (2005) 191–226.
[9] I.W. Hamley, Ordering in thin films of block copolymers: fundamentals to potential applications, Prog. Polym. Sci. 34 (11) (2009) 1161–1210.
[10] J. Hahn, V. Filiz, S. Rangou, B. Lademann, K. Buhr, J.I. Clodt, A. Jung, C. Abetz, V. Abetz, PtBS-*b*-P4VP and PTMSS-*b*-P4VP isoporous integral-asymmetric membranes with high thermal and chemical stability, Macromol. Mater. Eng. 298 (12) (2013) 1315–1321.
[11] S.Y. Yang, I. Ryu, H.Y. Kim, J.K. Kim, S.K. Jang, T.P. Russell, Nanoporous membranes with ultrahigh selectivity and flux for the filtration of viruses, Adv. Mater. 18 (6) (2006) 709–712.
[12] S.Y. Yang, J. Park, J. Yoon, M. Ree, S.K. Jang, J.K. Kim, Virus filtration membranes prepared from nanoporous block copolymers with good dimensional stability under high pressures and excellent solvent resistance, Adv. Funct. Mater. 18 (9) (2008) 1371–1377.
[13] W.A. Phillip, M. Amendt, B. O'Neill, L. Chen, M.A. Hillmyer, E.L. Cussler, Diffusion and flow across nanoporous polydicyclopentadiene-based membranes, ACS Appl. Mater. Interfaces 1 (2) (2009) 472–480.

[14] W.A. Phillip, B. O'Neill, M. Rodwogin, M.A. Hillmyer, E.L. Cussler, Self-assembled block copolymer thin films as water filtration membranes, ACS Appl. Mater. Interfaces 2 (5) (2010) 847–853.
[15] E.A. Jackson, Y. Lee, M.A. Hillmyer, ABAC tetrablock terpolymers for tough nanoporous filtration membranes, Macromolecules 46 (4) (2013) 1484–1491.
[16] K.-V. Peinemann, V. Abetz, P. Simon, Asymmetric superstructure formed in a block copolymer via phase separation, Nat. Mater. 6 (12) (2007) 992–996.
[17] S.P. Nunes, R. Sougrat, B. Hooghan, D.H. Anjum, A.R. Behzad, L. Zhao, N. Pradeep, I. Pinnay, U. Vainio, K.-V. Peinemann, Ultraporous films with uniform nanochannels by block copolymer micelles assembly, Macromolecules 43 (19) (2010) 8079–8085.
[18] D.S. Marques, U. Vainio, N.M. Chaparro, V.M. Calo, A.R. Bezahd, J.W. Pitera, K.-V. Peinemann, S.P. Nunes, Self-assembly in casting solutions of block copolymer membranes, Soft Matter 9 (23) (2013) 5557–5564.
[19] R. Hilke, N. Pradeep, P. Madhavan, U. Vainio, A.R. Behzad, R. Sougrat, S.P. Nunes, K.-V. Peinemann, Block copolymer hollow fiber membranes with catalytic activity and pH-response, ACS Appl. Mater. Interfaces 5 (15) (2013) 7001–7006.
[20] M. Radjabian, J. Koll, K. Buhr, U.A. Handge, V. Abetz, Hollow fiber spinning of block copolymers: influence of spinning conditions on morphological properties, Polymer 54 (7) (2013) 1803–1812.
[21] S. Rangou, K. Buhr, V. Filiz, J.I. Clodt, B. Lademann, J. Hahn, A. Jung, V. Abetz, Self-organized isoporous membranes with tailored pore sizes, J. Membr. Sci. 451 (2014) 266–275.
[22] Y. Wang, C. He, W. Xing, F. Li, L. Tong, Z. Chen, X. Liao, M. Steinhart, Nanoporous metal membranes with bicontinuous morphology from recyclable block-copolymer templates, Adv. Mater. 22 (18) (2010) 2068–2072.
[23] Y. Wang, F. Li, An emerging pore-making strategy: confined swelling-induced pore generation in block copolymer materials, Adv. Mater. 23 (19) (2011) 2134–2148.
[24] Z. Wang, X. Yao, Y. Wang, Swelling-induced mesoporous block copolymer membranes with intrinsically active surfaces for size-selective separation, J. Mater. Chem. 22 (38) (2012) 20542–20548.
[25] J. Yin, X. Yao, J.-Y. Liou, W. Sun, Y.-S. Sun, Y. Wang, Membranes with highly ordered straight nanopores by selective swelling of fast perpendicularly aligned block copolymers, ACS Nano 7 (11) (2013) 9961–9974.
[26] W. Sun, Z. Wang, X. Yao, L. Guo, X. Chen, Y. Wang, Surface-active isoporous membranes nondestructively derived from perpendicularly aligned block copolymers for size-selective separation, J. Membr. Sci. 466 (2014) 229–237.
[27] W.A. Phillip, B. O'Neill, M. Rodwogin, M.A. Hillmyer, E.L. Cussler, Gas and water liquid transport through nanoporous block copolymer membranes, J. Membr. Sci. 286 (1–2) (2006) 144–152.
[28] B. Li, W. Liu, Z. Jiang, X. Dong, B. Wang, Y. Zhong, Ultrathin and stable active layer of dense composite membrane enabled by poly(dopamine), Langmuir 25 (13) (2009) 7368–7374.
[29] T. Yamamoto, T. Kimura, M. Komura, Y. Suzuki, T. Iyoda, S. Asaoka, H. Nakanishi, Block copolymer permeable membrane with visualized high-density straight channels of poly(ethylene oxide), Adv. Funct. Mater. 21 (5) (2011) 918–926.
[30] T. Thurn-Albrecht, J. Schotter, G.A. Kästle, N. Emley, T. Shibauchi, L. Krusin-Elbaum, K. Guarini, C.T. Black, M.T. Tuominen, T.P. Russell, Ultrahigh-density nanowire arrays grown in self-assembled diblock copolymer templates, Science 290 (5499) (2000) 2126–2129.
[31] C.C. Ho, A.L. Zydney, Theoretical analysis of the effect of membrane morphology on fouling during microfiltration, Sep. Sci. Technol. 34 (13) (1999) 2461–2483.
[32] X. Zhao, Y. Su, W. Chen, J. Peng, Z. Jiang, Grafting perfluoroalkyl groups onto polyacrylonitrile membrane surface for improved fouling release property, J. Membr. Sci. 415–416 (2012) 824–834.
[33] L. Chu, T. Yamaguchi, S. Nakao, A molecular recognition microcapsule for environmental stimuli-responsive controlled-release, Adv. Mater. 14 (5) (2002) 386–389.